SPE-179158-MS

Optimal Perforation Location and Limited entry design for Promoting Simultaneous Growth of Multiple Hydraulic Fractures

Cheng Cheng and Andrew P. Bunger, University of Pittsburgh; Anthony P. Peirce, The University of British Columbia

This paper was prepared for presentation at the SPE Hydraulic Fracturing Technology Conference held in The Woodlands, Texas, USA, 9–11 February 2016.

Abstract

The objective of achieving uniform stimulation of a reservoir through hydraulic fracturing from a horizontal well typically depends upon the ability to generate a uniform array of hydraulic fractures from multiple entry points. However getting all the hydraulic fractures in an array to grow simultaneously is a challenge. The challenge apparently arises not only due to reservoir variability, but also in a substantial part due to the stress interaction among growing hydraulic fractures. This phenomenon, referred to as a stress shadowing, inhibits the growth of inner fractures and favors the growth of outer fractures in the array. Recently, we created a new hydraulic fracture simulator which simulates the growth of an array of hydraulic fractures in 10^{-6}–10^{-5} of the computation time required for fully coupled 3D simulations of multiple parallel planar hydraulic fracture growth. Using a novel energetic approach to account for the coupling among the hydraulic fractures and through judicious use of asymptotic approximate solutions, the simulation enables designs reducing the negative effects of stress shadow by balancing the interaction stresses through non-uniform perforation cluster spacings. Furthermore, so-called limited entry approaches are thought to be capable of promoting greater uniformity among simultaneously growing hydraulic fractures as long as the number and diameters of the perforations in each cluster are appropriately designed. In order to enable such optimizations and designs, we add perforation loss into to the approximate, energy-based simulator. Our results show the potential of choosing the proper perforation diameter and number to double the fracture surface area generated by a given injected fluid volume though minimizing the negative effect of interaction. The usefulness of the new simulator is demonstrated by development of example limited entry designs and optimal spacings for different numbers of entry points.

Introduction

Hydraulic fracturing (HF) has become a vital technique in the oil and gas industry. Pressurized fluid creates fractures in a rock mass and carries granular proppant into these fractures, providing pathways of decreased resistance to flow and hence an increased flow of hydrocarbons from the reservoir formation towards the well. Essentially all horizontal wells in unconventional reservoirs are stimulated today by hydraulic fracturing in a sequential manner from the ″toe″ to the ″heel″ of the well (as discussed in e.g. Lecampion et al. 2015). Although such a multistage (with multiple clusters of perforation comprising the

reservoir entry point within each stage) technique has enabled tremendous success in previously uneconomical reservoirs, analysis of production logs over several basins tends to show that between 20 to 40 percent of perforation clusters do not contribute to production (Miller et al. 2011). One influential factor is believed to be the well-known phenomenon of ″stress shadowing.″ Stress shadowing refers to suppression of some hydraulic fractures as a result of the compressive stresses exerted on them by nearby hydraulic fractures e.g. (Abass et al. 2009; Fisher et al. 2004; Meyer and Bazan, 2011). In particular, a stress shadow effect occurs when spacing between entry points, typically perforation clusters, is small relative to the final fracture length and/or height. For example, consider one stage that includes three fractures. In this case, growth of the outer two fractures in the array would typically dominate while the growth of the interior fracture would be severely inhibited due to the elevated compressive stresses to which it is subjected relative to the outer fractures.

Recently, a model developed by Peirce and Detournay (2008) called ILSA (″Implicit Level Set Algorithm″) was extended to a parallel-planar HF model with full 3D elastic coupling between the simultaneously propagating fractures by Peirce and Bunger (2015). Although ILSA is a benchmark in this research area, implementing state of the art approaches to enable accurate calculations on very coarse meshes, the model can require a week or more to compute a single multi-fracture result on typical reservoir length and time scales. A new approximate model, named ″C2Frac″, requires only seconds. It achieves this rapid computation time through a novel approximation to the fully-coupled problem (see Cheng and Bunger, In Press). The main innovation is coupling the influence of the stress shadow through the impact on the overall energy balance of the system. By then approximating the stress interactions, through asymptotic expansions of known analytical elastic crack solutions, the computations avoid full elastic field calculations. Through further approximation using asymptotic solutions for a penny-shaped fluid-driven fracture in an impermeable rock by Savitski and Detournay (2002), the model eventually determines the crack aperture $W_i(t)$, the net pressure $P_i(t)$, the fracture radius $R_i(t)$, and the inflow rate $Q_i(t)$ as a function of the fracture number i and pump time t for different choices of uniform or non-uniform inter-fracture spacing among N fractures. By drastically reducing the computation time while capturing the essential behavior of the system, with a useful level of accuracy compared to fully-coupled benchmarks provided by ILSA, C2Frac enables optimization of completions requiring hundreds or thousands of model evaluations.

The published energy-based ″C2Frac″ model (Cheng and Bunger, In Press), however, does not account for pressure loss through the perforations. This addition, presented here, comprises an important next step. Perforation pressure drop can be utilized to promote uniform, simultaneous hydraulic fracture growth (e.g. Lecampion and Desroches, 2015), noting these so-called ″limited entry″ methods draw inspiration and nomenclature from decades of experience in multi-zone stimulation from vertical wells (e.g. Howard and Fast, 1970).

Before continuing it is important to point out that one of the key unresolved issues in the background of the discussion running through this paper is what is meant by ″optimized″. The practically-relevant answer relates a measure of productivity of the well to a measure of the inputs such as materials and associated costs. This metric is not clearly defined and would vary depending on business objectives associated with a well. But even if this metric were well defined, until our model is coupled to a reservoir simulator, production cannot be predicted. As a result, optimization cannot, yet, directly be carried out in terms of production. Nonetheless, in order to demonstrate the capacity for optimization and to provide a first pass at predicting a production-optimizing configuration, here we will adopt the fracture surface area as our metric of the effectiveness of a stimulation. The surface areas will be compared at the same volume of injected fluid – hence we can also think of these to be cases with the same total mass of proppant placed. Under these circumstances we propose that maximizing fracture surface area is a reasonable objective because it scales to production both in classical treatments of production from hydraulic fractures (see e.g. Economides and Nolte, 2000, chapter 1) and in more recent approaches relating

Stimulated Reservoir Volume (SRV) to production (e.g. Fisher et al., 2002). (Noting that SRV was originally defined based on the geometry of microseismic clouds (Warpinski et al., 2005) but, to have a direct connection to forecasted production, must essentially correspond to the area of hydraulic fractures times the characteristic width of the region of drainage around the hydraulic fractures.)

Here we begin by introducing the modeling approach and demonstrating the capability and limitations for matching benchmark solutions provided by the fully-coupled planar 3D simulator ILSA. We then show how perforation loss is incorporated via the global energy balance and, in turn, how the algorithm underlying the C2Frac simulator is built on this global energy balance. Then through numerical experiments, we illustrate cases for uniform and non-uniform perforation and spacing designs. As a result, we utilize the C2Frac model to search for the optimized perforation design, providing examples of optimized designs for five fractures and six fractures per stage. We conclude with a discussion of the benefits of optimization and the complimentary nature of limited entry and non-uniform fracture spacing as approaches for promoting multiple hydraulic fracture growth.

Geometry and Propagation Regimes

The model considers that a viscous fluid is injected from a horizontal wellbore. The hydraulic fractures are assumed to initiate and grow transversely to the well, propagating perpendicularly to the minimum *in situ* confining stress σ_{min} (see Fig. 1). The fluid, injected at a total volumetric rate $Q(t)$, is partitioned dynamically, i.e. as a part of the transient solution to the coupled problem, to the N perforation clusters distributed within one stage of length Z. The spacing $h_{i,i+1}$, i-$1,\ldots,N$-1 is the distance between fracture i and fracture $i+1$ as depicted in Fig. 1. Hence,

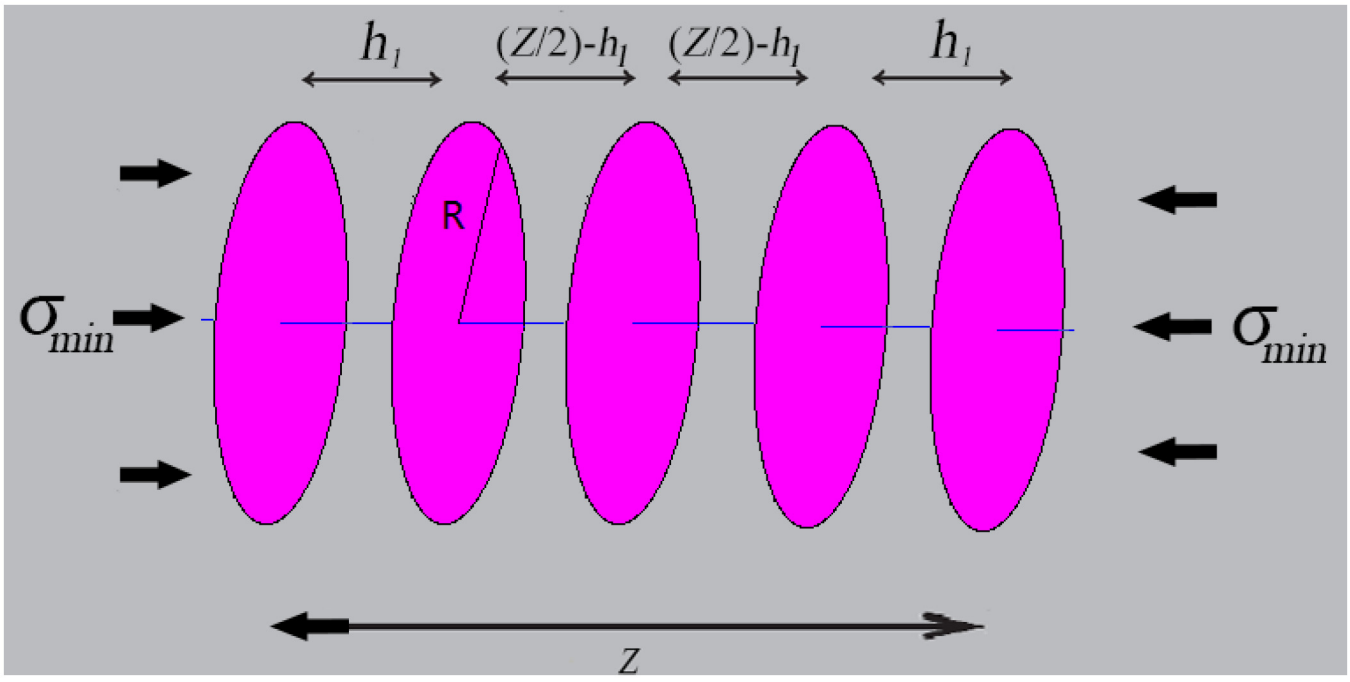

Figure 1—Geometric configuration of a hydraulic fracturing stage of length Z with a symmetric array of 5 hydraulic fractures.

$$Z = \sum_{i=1}^{N-1} h_{i,i+1} \tag{1}$$

During the entire period of growth, the fractures are assumed to remain planar and radial, centered on the wellbore for which the radius is denoted R_w. This idealization neglects: a) deviation of the fracture path

which could result from the presence of a height growth barrier leading to a transition to so-called ″PKN″ or blade-like geometry (Perkins and Kern, 1961; Nordgren, 1972), and b) path deflections due to interactions with natural fractures, or the stresses induced by previously-placed hydraulic fractures (Roussel and Sharma, 2010,2011; Bunger et al., 2012; Sesetty and Ghassemi, 2013; Wu and Olson, 2013; Daneshy, 2015). In essence this radial planar assumption is valid provided: 1) the final fracture length is similar to the height as limited by barriers to vertical growth, and 2) the difference between the minimum and maximum horizontal stresses is sufficiently large (see extended discussion in Peirce and Bunger, 2015). We note, however, that transition to PKN geometry and gradual curving of the fracture paths due to stresses induced by their neighbors can, in principle, be accounted for readily as an extension to the model presented here.

The radially-growing, planar hydraulic fractures are therefore considered to be driven by an incompressible Newtonian fluid through a homogeneous, impermeable, brittle elastic rock. The fluid is thus characterized by its dynamic viscosity (μ). The rock is characterized by fracture toughness (K_{IC}), Young's modulus (E), and Poisson's ratio (ν). Note that accounting for fluid leakoff to the rock, heterogeneity of in situ stress, variable rock strength, and/or modeling other fluid rheology is a relatively straightforward as an extension to the present work that is nonetheless beyond the present scope.

Prior Development of the Model

The benchmark ILSA II model utilizes a parallel-planar 3D model incorporating full elastic-hydrodynamic coupling to account for the fracture interactions (Peirce and Bunger, 2015, extending the original ILSA model of Peirce and Detournay, 2008). However, in spite of a novel algorithm enabling accurate calculation on extremely coarse meshes (see the comparative convergence study in Lecampion et al., 2013, for details), it is time consuming. The goal, then, of the new, so-called C2Frac model is to discern and develop the most rapidly-computing model with the capability to obtain useful results that can be used for optimization of hydraulic fracture stage design, i.e. a reasonably accurate indication of fluid partitioning to each entry point, fracture length, and/or of the overall fracture surface area generated by a given treatment. The result of the initial effort is a model capable of approximating multiple hydraulic fracture growth solutions over limited ranges but within 10^{-6}–10^{-5} of the time required for the full simulations, that is, within seconds instead of days or weeks (Cheng and Bunger, In Press).

The algorithm used in C2Frac will be explained in greater detail subsequently, in the context of expanding the algorithm to include pressure drop across the perforations. However, it is useful to reiterate the results of model benchmarking carried out by Cheng and Bunger (2015), as these illustrate the current limitations of C2Frac. The benchmarking is carried out with C2Frac and ILSA II. A case with 5 non-uniformly-spaced hydraulic fractures, presented in Fig. 2, illustrates the main result. Note that ″outer″ refers to fractures 1 and 5, which are identical by symmetry of this particular case. Similarly ″inner″ refers to fractures 2 and 4, with ″middle″ referring to the central fracture (number 3). It is here shown that: 1) C2Frac approximates ILSA II with a 10%-20% discrepancy in fluid influx to each fracture, 2) the crack length and wellbore pressure agrees within in a few percent, and 3) the fracture width at the wellbore is well approximated for the outer fractures and is estimated within a factor of 2 for the inner and middle fractures. It is worthwhile to note here that the current level of mismatch in the inlet fracture width could be problematic for predicting screenout; ongoing work is aimed at improving the width prediction and quantifying the impact of the mismatch on screenout predictions when proppant transport is included in the model.

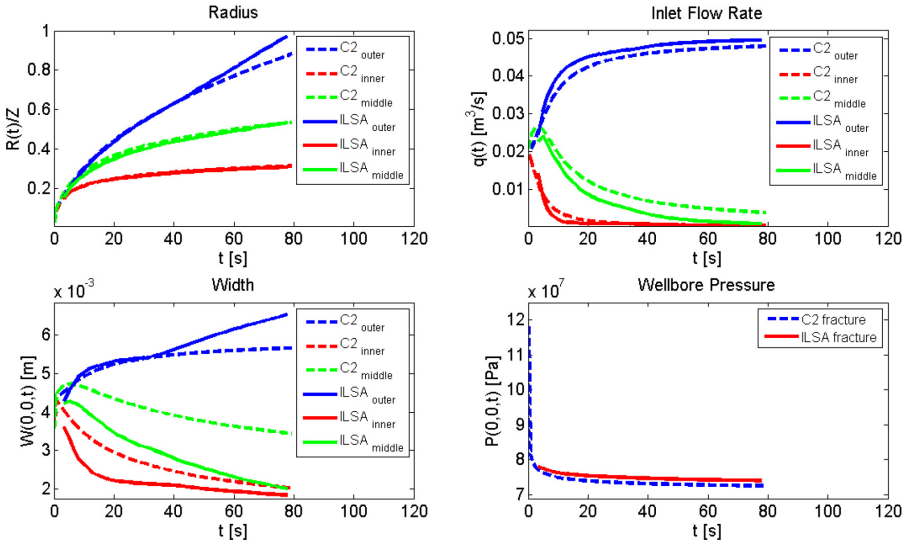

Figure 2—C2Frac results for non-uniformly spaced fracture array (h1 = 4.0 m, hence spacings of 4m, 6m, 6m, and 4m among fractures) compared with the ILSA II benchmark, after Cheng and Bunger (In Press). C2Frac matches the benchmark radius, influx, and pressure very well until the largest fracture approaches 0.6 times the total span of the array, Z.

To continue the benchmarking comparison, in Fig. 3, the approximation of the total generated fracture surface area is verified relative to the benchmark solution. Recall that total fracture area is potentially useful because it is one possible metric one may chose for optimization. This comparison clarifies the limits of the current approximations utilized by C2Frac, namely that the solution diverges from the benchmark beyond the point where the radius of the largest fracture is more than 0.6 times the length (Z) of the fracture array (stage). This is expected because the stress interactions among the fractures use far-field approximations, valid when the fracture spacing is large enough relative to the fracture radius. While future efforts are aimed at developing and employing a uniform approximation for the stress interactions that will alleviate this limitation, here we will maintain the far field approximation and generalize to include perforation losses. It is important, then, to realize two things from this discussion: 1) the current C2Frac and its results presented subsequently is valid when the radius of the largest fracture is less than about 0.6 times the span of the array, and 2) this is not an intrinsic limitation to the energy-based algorithm of C2Frac but rather it arises because of the approximation of the interaction stress, which will be alleviated in future versions of the model.

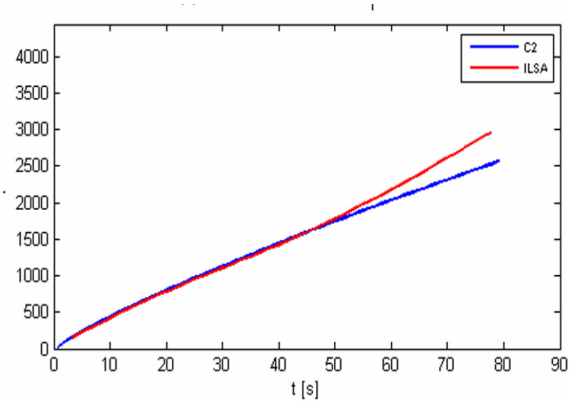

Figure 3—C2Frac results compared with ILSA on Total fractured area A_{total} (t, h_1) for a five fracture array with non-uniform spacing of 4m, 6m, 6m, and 4m between fractures, after Cheng and Bunger (In Press). C2Frac matches the benchmark very well until the longest fracture exceeds about 0.6 times the span of the array.

Limited entry

In order to consider limited entry design, the perforation loss is included into C2Frac via its contribution to the global energy balance equation (after Bunger 2013, Bunger et al. 2014)

$$P_i Q_i = \sigma_{min} Q_i + \left(\dot{U} - \dot{W}_I + \dot{F}_c + \dot{F}_f + \dot{F}_{perf} \right) \tag{2}$$

where the left hand side is the rate of energy input to the i^{th} fracture, the first term on the right hand side represents the energy required to open the fracture against the *in situ* confining stress, and $\{U, W_I, F_c, F_f, F_{perf}\}$ relate to the increase in elastic strain energy, the work exerted on the hydraulic fracture via the stresses induced by its neighbors, the energy dissipation associated with rock breakage, the energy dissipated in viscous fluid flow, and the energy dissipated due to flow through the perforations, respectively.

The energy quantities required to compute Eq. (2) are defined in Bunger (2013) and implemented in C2Frac with a detailed account in Cheng and Bunger (In Press), and therefore will not be reiterated here. Instead we focus on the main innovation, which is the inclusion of perforation loss. Accounting for perforation loss makes use of the analysis of the pressure drop as fluid flows through a cluster of n perforation holes (Crump and Conway 1988, Economides and Nolte 2000), see Fig. 4. This classical result gives rise to an expression for the power loss through the i^{th} entry point (Bunger et al, 2014)

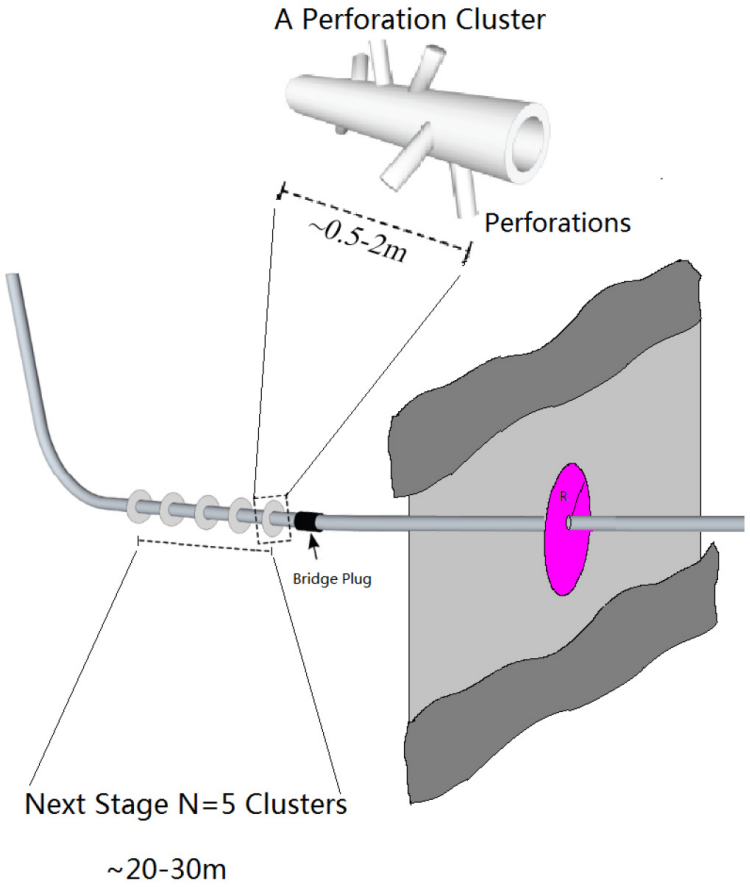

Figure 4—Sketch of perforation clusters, modified from Lecampion and Desroches (2015).

$$\dot{F}_{perf} = \left(\frac{a\rho}{n^2 D_p^4 C^2} \right) Q_i(t)^3 \tag{3}$$

Each cluster has n perforations; usually this value is within the range of 5 to 20, and it ideally should be the number of holes that actually accommodate the fluid flow into the hydraulic fracture, not just the total number placed (some of which may be plugged or otherwise ineffective). Here also D_p represents the perforation diameter, which is usually within a range from 6 to 15 mm (about ¼ to 5/8 inches). As before, Q_i(t) represents the injection rate to the i^{th} fracture, which will vary with the pumping time t (recall Fig. 2). There is also a shape factor for the perforation tunnels themselves, given here by C which is typically taken as 0.56 before erosion (sharp perforation) and 0.89 after erosion based on the experimental results of Crump and Conway (1988). In C2Frac perforation erosion is neglected so C is taken as a constant equal to 0.56. The numerical factor, a, is usually taken from Crump and Conway (1988) as 0.8106. The fluid injected into the reservoir has a fluid density of ρ. Taken together, the bracketed quantities in Eq. (2) comprise a coefficient of proportionality between the power loss associated with flow through the perforations and the cube of the flow rate.

With the addition of pressure, and hence energy, loss through the perforations, the solution algorithm from Cheng and Bunger (In Press) is modified as follows:

1. User inputs: Set values for the physical parameters $\{E, \nu, K_{IC}, \mu, Q, Z, \sigma_{min}, R_w, h_{i,j}\}$as well as the initial time, final time, and time step for the calculation, $\{t_0; t_f; \Delta t\}$, respectively.
2. Initial state: Set $t = t_0$ and assume initially uniform influx, $Q_i^{(0)} = Q/N$. Estimate the width, pressure (which also approximates the inlet pressure), and length of each hydraulic fracture (i = 1,. . ., N) according to the solution for a viscosity-dominated hydraulic fracture presented by Savitski and Detournay (2002), but with small adjustments to the coefficients demonstrated by Cheng and Bunger (2015) to give closer approximation to the benchmark solution for multiple interacting hydraulic fractures. Hence,

$$w_i^{(0)} = 0.95 \left(\frac{\mu'^2 \left(Q_i^{(0)}\right)^3 t_0}{E'^2} \right)^{1/9} \quad w_i^{(0)} = 0.7349 \left(\frac{E' \left(Q_i^{(0)}\right)^3 t_0^4}{\mu'} \right)^{1/9} \quad P_i^{(0)} = \sigma_{min} + \left(\frac{\mu' E'^2}{t_0} \right)^{1/3} \tag{4}$$

3. Begin time step loop: Advance to the k time step, $t^{(k)} = t^{(k-1)} + \Delta t$. Update mean influxes according to

$$\left\langle Q_i \right\rangle^{(k)} = \frac{1}{t^{(k-1)}} \int_0^{t^{(k-1)}} Q_i dt, \qquad i = 1,\ldots,N \tag{5}$$

Note the integral is evaluated numerically using the trapezoid rule with previously-computed values of $Q_i^{(0)}$, . . ., $Q_i^{(k-1)}$.

4. Use non-linear solver (e.g. Matlab ″fsolve″) to obtain the N influxes $Q_i^{(k)}$ simultaneously satisfying the constraints that the pressure at the inlet of all of the fractures is the same (i.e. connected by a horizontal wellbore with negligible friction loss along the wellbore between the entry points) and a further constraint that the sum of all influxes to the fractures must equal the total influx to the well. That is,

$$P_1^{(k)} = P_2^{(k)} = \ldots = P_N^{(k)}, \qquad Q = \sum_{i=1}^{N} Q_i^{(k)}, \tag{6}$$

Here a critical point is that the pressures are estimated using the energy balance equation via Eq. (2). Upon substitution of the estimates for the power terms this estimate is

$$P_i^{(k)} = \sigma_{min} + \frac{1}{Q_i^{(k)}} \left[\begin{array}{l} -0.06215 \left(\dfrac{E'^2 \left(\langle Q_i \rangle^{(k)} \right)^3 \mu'}{t^{(k)}} \right)^{1/3} - \ldots \\ 0.03420 E' \langle Q_i \rangle^{(k)} \sum_{j=1}^{N, j \neq i} \dfrac{w_j^{(k-1)} \left[min\left(R_j^{(k-1)}, R_i^{(k-1)} \right) \right]}{h_{i,j}^3} - \ldots \\ 0.04637 \left(\dfrac{E'^2 \mu' \left(\langle Q_i \rangle^{(k)} \right)^3}{t^{(k)}} \right)^{1/3} ln \left(\dfrac{R_w^9 \mu'}{E' \left(\langle Q_i \rangle^{(k)} \right)^3 \left(t^{(k)} \right)^4} \right)^{1/9} + \ldots \\ 0.2136 \left(\dfrac{E'^2 \mu' \left(\langle Q_i \rangle^{(k)} \right)^3}{t^{(k)}} \right)^{1/3} \\ \left(\dfrac{a\rho}{n^2 D_p^4 C^2} \right) \left(\langle Q_j \rangle^{(k)} \right)^3 \end{array} \right] \tag{7}$$

The specific terms in the energy-based pressure equation come from carrying out the energy integrals upon substitution of approximations for the width, pressure, and radius coming from the single, viscosity-dominated solution of Savitski and Detournay (2002) with a far field asymptotic solution for the interaction stress also entering via the work of interaction term, W_I. Hence, the main change is addition of the final term quantifying the energy loss through the perforations. Note the simplicity of the modification, illustrating the potential to include other mechanisms (e.g. fluid leakoff) in a straightforward manner provided their contribution to the global energy balance can be computed.

5. Update width and radius of each hydraulic fracture ($i = 1, \ldots, N$), again using the viscosity-dominated asymptotic solution of Savitsky and Detournay (2002) with a small adjustment of the coefficients found by Cheng and Bunger (2015) to improve the match to the benchmark solution for multiple interacting fractures. Hence,

$$w_i^{(k)} = 0.95 \left(\frac{\mu'^2 \left(Q_i^{(k)} \right)^3 t^{(k)}}{E'^2} \right)^{1/9}, \quad R_i^{(k)} = 0.7349 \left(\frac{E' \left(Q_i^{(k)} \right)^3 \left(t^{(k)} \right)^4}{\mu'} \right)^{1/9} \tag{8}$$

6. Repeat steps (3)-(5) until $t^{(k)} = t_f$.

Limited Entry Design

Limited entry design refers to manipulation of the pressure loss through each perforation cluster by varying the perforation diameter D_p and/or the number of perforation holes, n (Bunger et al., 2014). One proposed approach to promoting simultaneous HF growth entails using smaller/fewer holes for the outer fractures and more/larger holes for the inner fractures within an array in order to counteract the stress shadow-driven suppression of the inner fractures (Lecampion and Desroches, 2015).

In what follows, the limited entry design approach is explored using C2Frac. Two types of cases are considered. The first is the uniform perforation case with same perforation diameter and number for all clusters, exploring how uniform reduction of the number and/or diameter of the perforation holes can promote simultaneous hydraulic fracture growth. Second, using results from the first step, non-uniform limited entry cases are explored by changing D_p and n in different clusters. Specifically we show how

non-uniform limited entry can be used in conjunction with non-uniform spacing to obtain an optimized spacing (in terms of created fracture surface area) that is closer to uniform spacing than it would be without the use of limited entry. After presented these cases, we compare the optimal and non-optimal designs to demonstrate the potential benefits of simultaneous and complimentary use of fracture spacing optimization combined with limited entry design.

Design Type #1: Uniform Limited Entry

The first type of design considers uniform limited entry, that is, the restrictions are engineered but constrained such that all clusters have the same number and diameter of perforation holes. Noting an equivalence between reducing the number of perforation holes per cluster and reducing the square of the diameter of the perforation holes (Eq. 3), it suffices to firstly fix the number of perforation holes, n, to be constant and equal to 20. This assumption corresponds to maximum value in the range of 5 and 20. Next, C2Frac is used to simulate how the total fracture area varies with the perforation diameter, D_p. The remaining parameters are defined in Table 1.

Table 1—Base parameter values, used in all examples unless otherwise noted.

Parameter	Value
E	9.5 GPa
n	0.2
K_{IC}	0
μ	1 Pa s
Q	0.1 m3/s
Z	20 m
σ_{min}	70 MPa
R_w	0.2 m
ρ	1000 kg/m3
a	0.8106
C	0.56
n	20

The results indicate when the perforation diameter is smaller (at the same n in every cluster), more fracture area and a more uniform stimulation can be obtained, as shown in Fig. 5. Moreover, the benefit is apparent at any perforation spacing. In addition, the maximum point of the curves moves closer to 5m, which is the uniform spacing in this test case. The impact of changing the number of perforations is similar (Fig. 6), as expected due to the appearance of both n and D_p in the perforation loss Eq. (3). Similar to Fig. 5, fewer perforation holes per cluster increases the pressure loss through the perforations at a given flow rate, thereby driving a more uniform distribution of fluid among the entry points and resulting in more generated fracture area. It is also important to note that the optimal spacing in terms of maximizing the fracture area is closer to uniform (h_1=5m is the uniform spacing configuration in these 5 fracture cases, recall Fig. 1). There is, however, a tradeoff because the net pressure, and therefore the required pumping power, is increased by limited entry design. For example, with uniform spacing and in reference to varying n (Fig. 6), the net pressure increases by over 60% when n is reduced from 20 to 10 and by a further nearly 50% when n is reduced from 10 to 5. This corresponds to an increase of several, and up to 4 MPa in required fluid pressure (hundreds and up to 600 psi). The greatest impact on generating more fracture area from a more uniform spacing of fractures is obtained with n=1, representing over a factor of 10 increase in net pressure when compared with the n=20 cases.

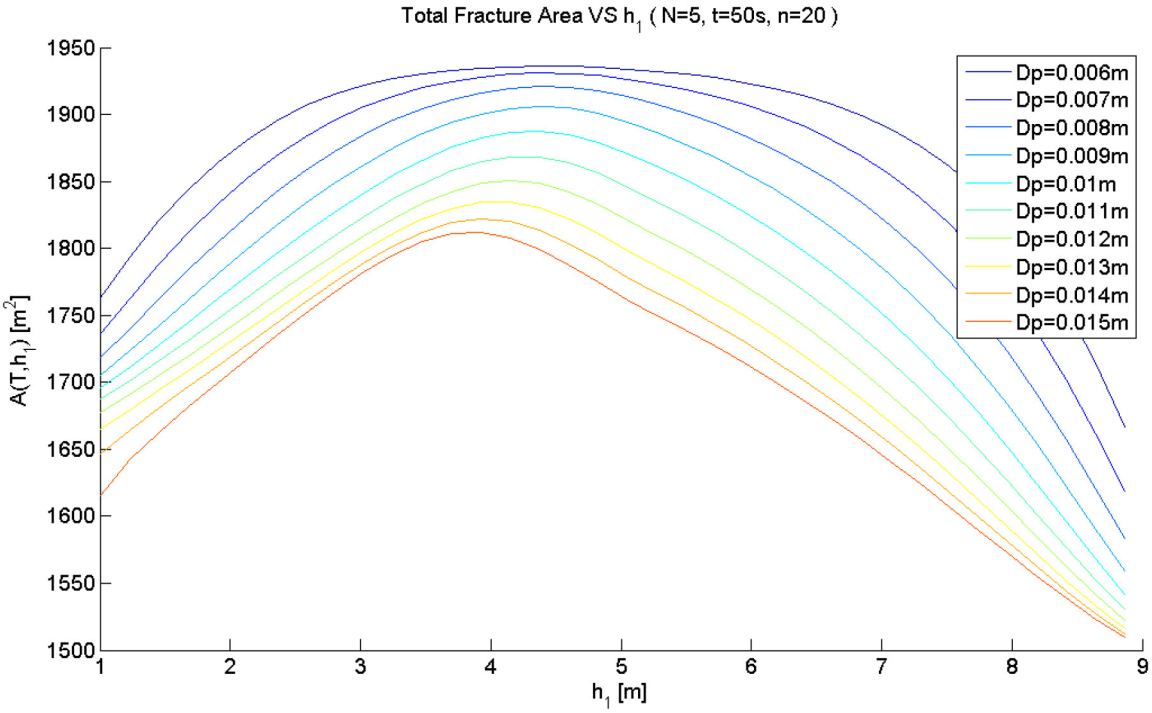

Figure 5—Total fractured area dependence on different perforation diameter D_p (at 50s). Increasing the perforation friction by decreasing the perforation hole diameter increases the generated fracture surface area and causes the optimal fracture spacing to be closer to uniform (h_1=5m in this example is uniform spacing).

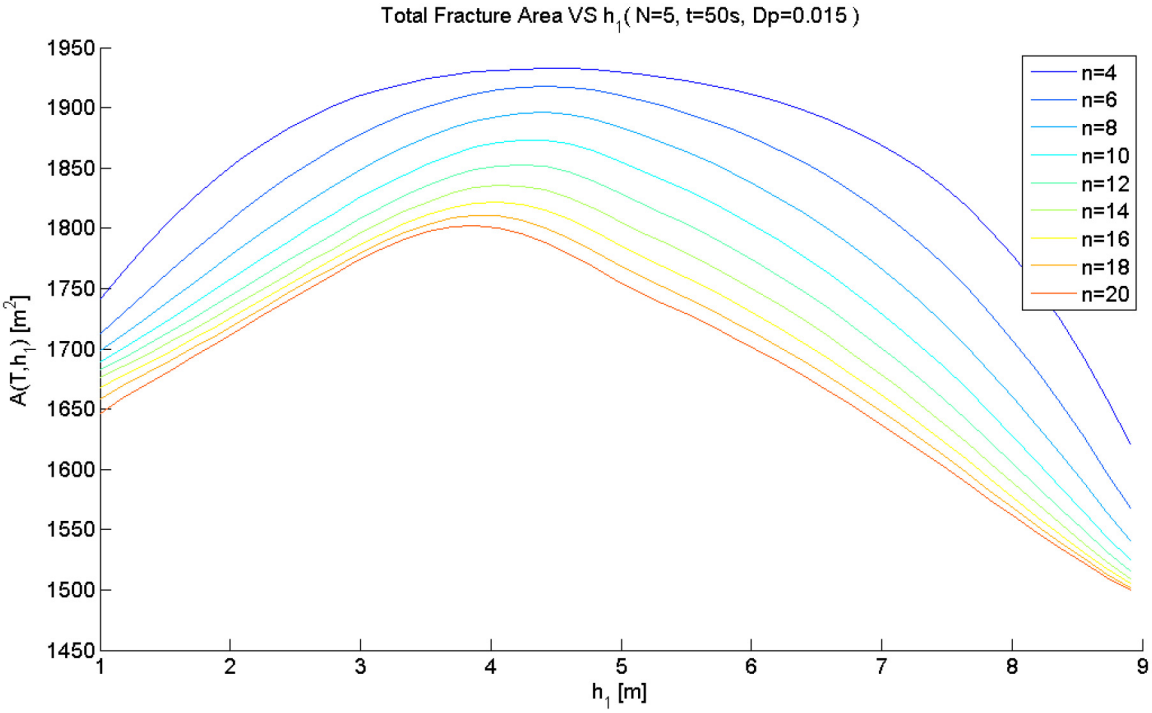

Figure 6—Total fractured area dependence on different perforation hole number n (at 50s). Increasing the perforation friction by decreasing the number of perforation holes increases the generated fracture surface area and causes the optimal fracture spacing to be closer to uniform (h_1=5m in this example is uniform spacing).

We can similarly explore the impact of uniform limited entry on the uniform spacing case by selecting the uniform spacing h_1=5m and varying the perforation diameter from 6mm to 15mm, with results shown

in Fig. 7. Initially, when all the fractures are small, the perforation diameter influence is insignificant. However, as treatment time increases, the smaller perforation diameter case generates more new fracture area because it drives more uniform distribution of fluid among the fractures. At the early times C2Frac can simulate, the impact of decreasing the perforation diameter is around 5–10%. However, the results are diverging and the benefit is expected to increase with time. Naturally the continuation of this trend will be examined with future versions of C2Frac that are free of the restriction on applicability of results arising from the current far field stress interaction approximation.

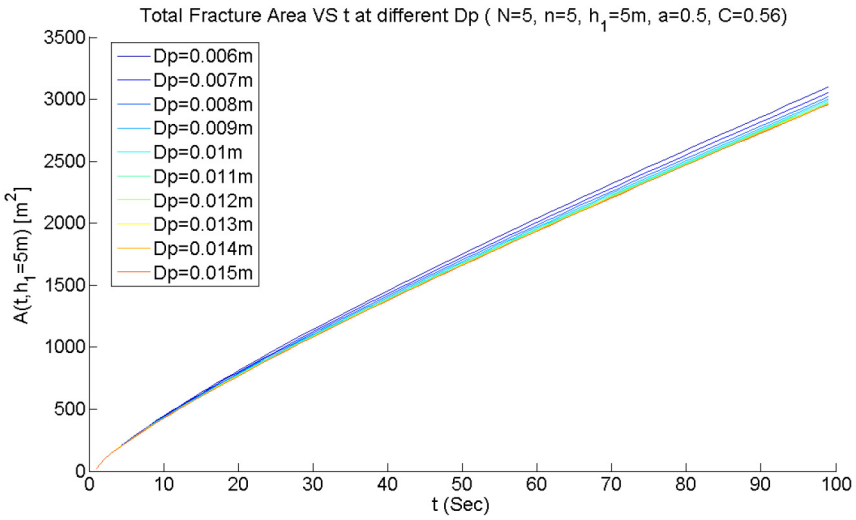

Figure 7—Increasing the perforation friction by decreasing the perforation diameter leads to greater fracture surface area for the same pumped volume, with the differences among the cases increasing with time.

A practical question arises from these results. If one is given a desired spacing (i.e. defined for a symmetric 5 fracture array by h_1), then what is a combination of n and D_p that will generate the greatest fracture surface area? Or, one may similarly ask what is the spacing and number of perforations required to optimize the fracture area for a fixed perforation diameter? These questions are addressed in Fig. 8. Firstly, it is shown by contrasting Fig.8a-b that the best configuration depends upon the time of pumping at which the area is to be maximized. Utilizing the same perforation diameter and a smaller perforation number is found to result in optimized h_1 that is closer to 5m, corresponding to uniform spacing in this example. Regardless of the perforation number, all the curves converge at small and large diameters – i.e. in the limits of infinite and zero perforation pressure loss.

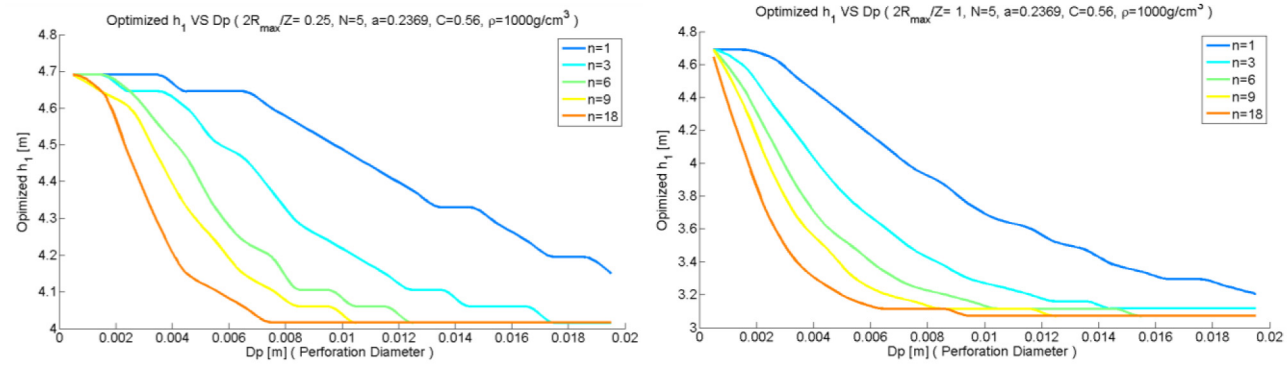

a) b)

Figure 8—Optimized fracture spacing depending on perforation diameter D_p and n at a) 5s, and b) 50s.

Design Type #2: Non-Uniform Limited Entry

Previously, non-uniform spacing was shown to provide larger fracture surface area by mitigating the impact of stress shadow (Peirce and Bunger 2015). Similarly, we predict that the non-uniform design for perforations should also generate more fracture surface area than the uniform perforation design – and, in fact, previous studies have also predicted this to be the case (Lecampion and Desroches, 2015). C2Frac is used to examine the potential benefit of non-uniform limited entry design, that is, a design that varies the number and/or diameter of perforations for each perforation cluster, typically energetically penalizing the outer clusters with smaller/fewer holes and promoting the central clusters with more/larger holes.

To reduce the number of degrees of freedom, perforations in inner and middle clusters are taken to be the same as each other but different from the outer clusters. First n is fixed at 20 and simulations (hundreds) are performed to show the variation of the fracture surface area with h_1 and D_p (Fig. 9). In Fig. 9(a), the perforation diameter of the outer clusters is the same (0.006m) for each case while the inner and middle clusters varied from 0.006 to 0.015m. Fig. 9(b) holds the middle and inner diameter at 0.006 m while varying the diameter of the outer fractures from 0.006 to 0.015m. If the perforation diameter of the outer cluster is smaller in relation to the inner and middle, a larger fracture area can be generated with uniformly-spaced clusters. The trend becomes more obvious as the difference in the diameters increases.

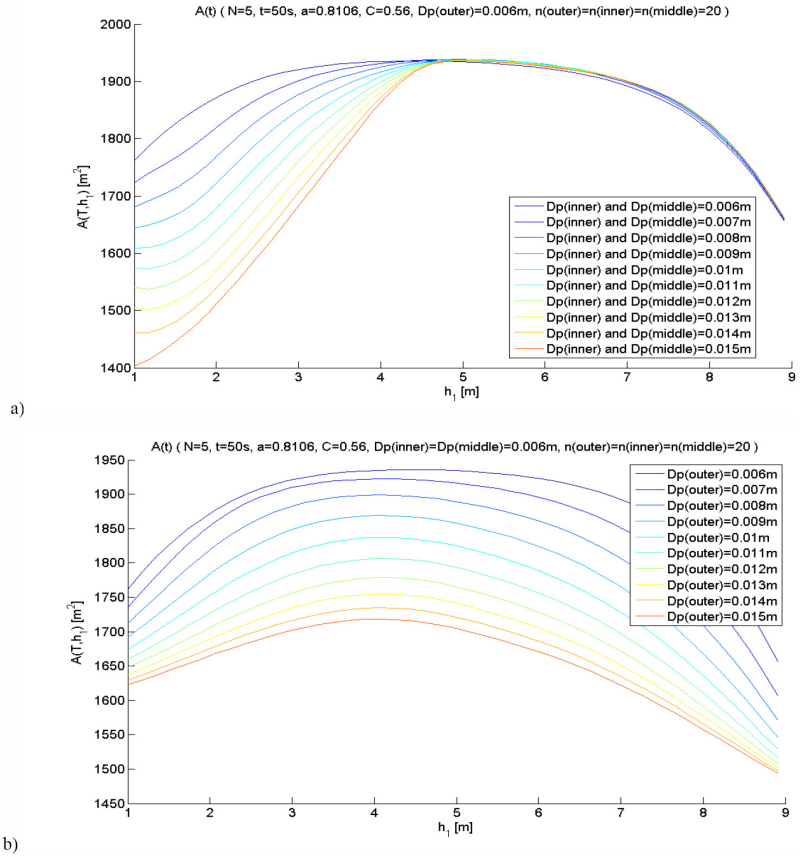

Figure 9—Plot total fracture area evolution with h_1 at 50s with n=20. a) *Dp*(outer)=0.006m is held constant while varying the perforation diameter for the inner and middle fractures. b) *Dp*(inner) and *Dp*(middle) are held constant (0.006 m) while varying the perforation diameter for the outer fracture.

Next, we take D_p=15mm and investigate the impact of using different n for different clusters. In Fig. 10(a) the n of inner and middle cluster is the variable with n for the outer cluster fixed, while in Fig. 10(b) n is fixed for the inner and middle clusters while n for the outer cluster is varied. In Fig. 10(a) it is hard

to distinguish the differences among the cases. A small variation can be seen in Fig. 10(b) wherein a smaller value of n for the outer cluster leads to a slightly larger fracture area. The optimal choice for the perforations is $n=20$ for all clusters. But it is clear that varying the perforation diameter has a larger impact than varying the number of perforations. This is not surprising due to the larger power on D_p than on n in Eq. (3).

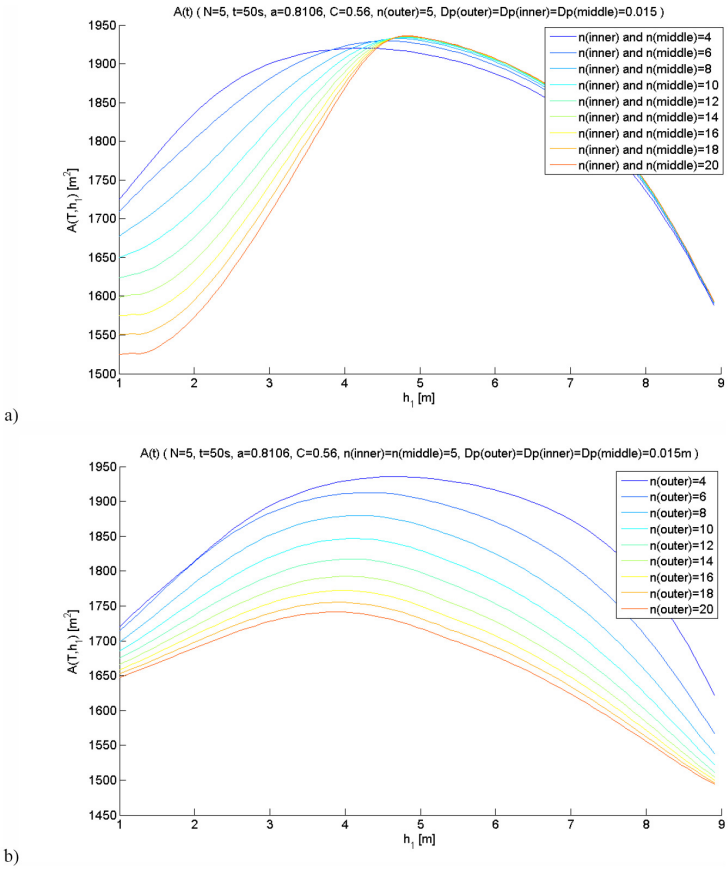

Figure 10—Plot total fracture area evolution with h_1 at 50s for the optimized *Dp* decribed before. a), *n*(outer) is constant. b), *n*(inner) and *n*(middle) is constant.

Discussion of Benefits of Optimization

Here we will examine the benefit of optimization, especially optimization that utilizes limited entry and non-uniform spacing in a complimentary way. Firstly we examine the case with $D_p=15$mm, n(outer)=5, n(inner)=n(middle)=20, which is found to provide an optimal result for the case of 5 uniformly-spaced fractures. Keeping the other parameters the same as before, Fig. 11 plots the total fracture area as a function of h_1 for different treatment times, with Fig. 11a showing the case where perforation friction is switched off by setting $a=0$ (see Eq. 3), while Fig. 11b shows the same case with $a=0.8109$ after Crump and Conway (1988). The first observation is that, for both cases, as the treatment time increases the value of h_1 that gives the greatest fracture area decreases. However, the rate at which it decreases is decreasing with time, suggesting that the optimum h_1 attains some asymptotic value at large time. This observation gives tentative support to using this model, in spite of its limitation to the early-time portion of the growth before the fractures get too long relative to their separation, because the optimal h_1 is expected to change by only a little after the time at which these simulations are stopped.

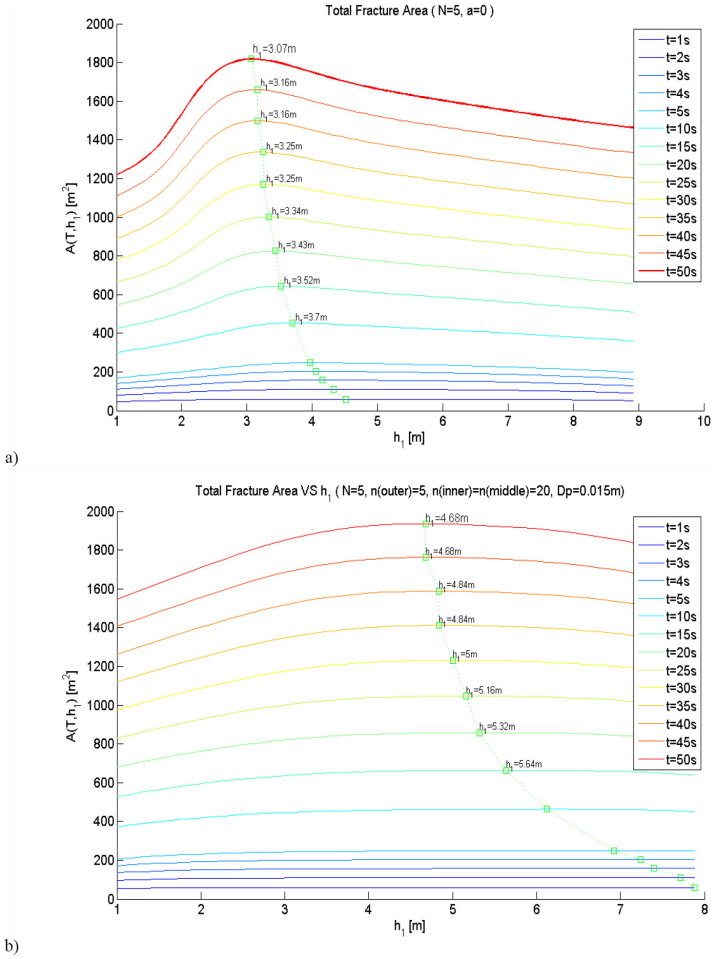

Figure 11—Total fracture area evolution with h_1 at different treating times, a) without perforation loss (having set a=0, see Eq. 2), b) the optimal perforation design.

A second relevant observation is that for both cases the difference in fracture surface area between the optimal case and the uniform spacing case (still h_1=5m) increases with time. There is no reason to suggest this trend would not continue; indeed Peirce and Bunger (2015) observe more than 50% difference between optimal and uniform spacing after 140 seconds pumping time for the same input parameters as are considered here but with growth contained to a 20m high reservoir. Hence these results suggest the benefits of optimization increase with increasing pumping time.

A third observation concerns the main difference between neglected perforation loss (Fig. 11a), and a case with optimized limited entry for uniform spacing, Fig. 11(b), namely that the line connecting the maximum points shifts the optimized values of h_1 closer to 5m. That is to say, when limited entry is used, optimal results can be obtained with closer-to-uniform spacing than when limited entry is not used. Presumably this could have a positive impact on production by making the stimulation more uniform along the well, although we also note there would be a cost in terms of increased net pressure and hence required pumping power. In this example the net pressure increase is a factor of 4 comparing the optimal-spacing limited entry design in Fig. 11(b) with the optimal spacing without limited entry case in Fig. 11(a).

Figure 12 further demonstrates the improvement of optimal perforation design. For this illustration, we select one non-optimized design with D_p=15mm (~5/8″), n=20 for all clusters and uniform spacing as a comparison case with no limited entry or spacing optimization. A comparison is then made among: a) this non-optimized case, b) a case with optimal spacing and non-optimized limited entry design, c) optimal

perforation with non-optimized space, and d) optimal spacing with limited entry. We can see from this comparison a growing advantage of the fully optimized case relative to the non-optimized case that reaches 15% already at 50 seconds into the treatment. The greatest advantage is provided by the fully optimized case, although the case with perforation optimization only is a close second, requiring about 30% higher net pressure (2 MPa or 300 psi) than the fully optimized case.

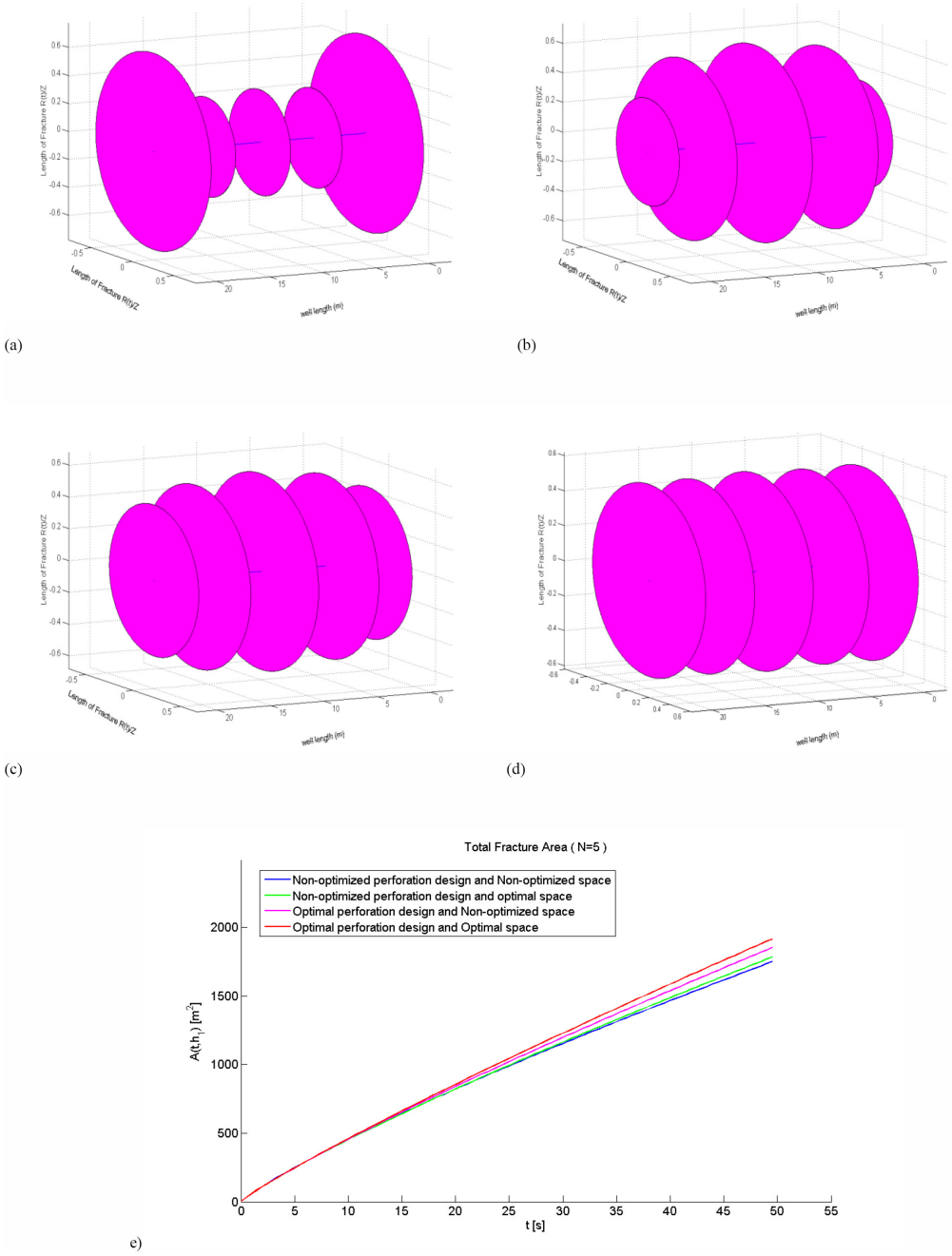

Figure 12—Growth geometry after 50s growth for: a) Non-optimized perforation design and non-optimized spacing, *h_1=5m, n=20, Dp=0.15*. b) Non-optimized perforation design with optimal spacing, *h_1=3.40m, n=20, Dp=0.15m*. c) Optimal perforation design with non-optimized spacing, *h_1=4m, n(outer)=5, n(inner)=n(middle)=20, Dp=0.015m*. d) Optimal perforation design with optimal spacing, *h_1=4.62m, n(outer)=5, n(inner)=n(middle)=20, Dp=0.015m*. e) The total fracture areas corresponding to cases a-d.

It is also useful to extend consideration to six fractures for the purpose of showing the potential for optimization over a larger number of design parameters. As an illustrative example, again based on

thousands of simulations that are practically enabled by the short computation times required by C2Frac, we show how perforation hole diameters impact fracture surface area after a fixed pumping time (i.e. for the same injected fluid volume). Figure 13a gives contours of the fracture area as a function of the number of perforation holes for the outer two fractures and for the central four fractures in a uniformly-spaced array (with D_p=6mm). Here we observe a band of combinations of numbers of perforations holes maximizing the fracture surface area. However, while the generated surface area does not vary by much through this band of combinations, the required net pressure does (Fig. 13b).

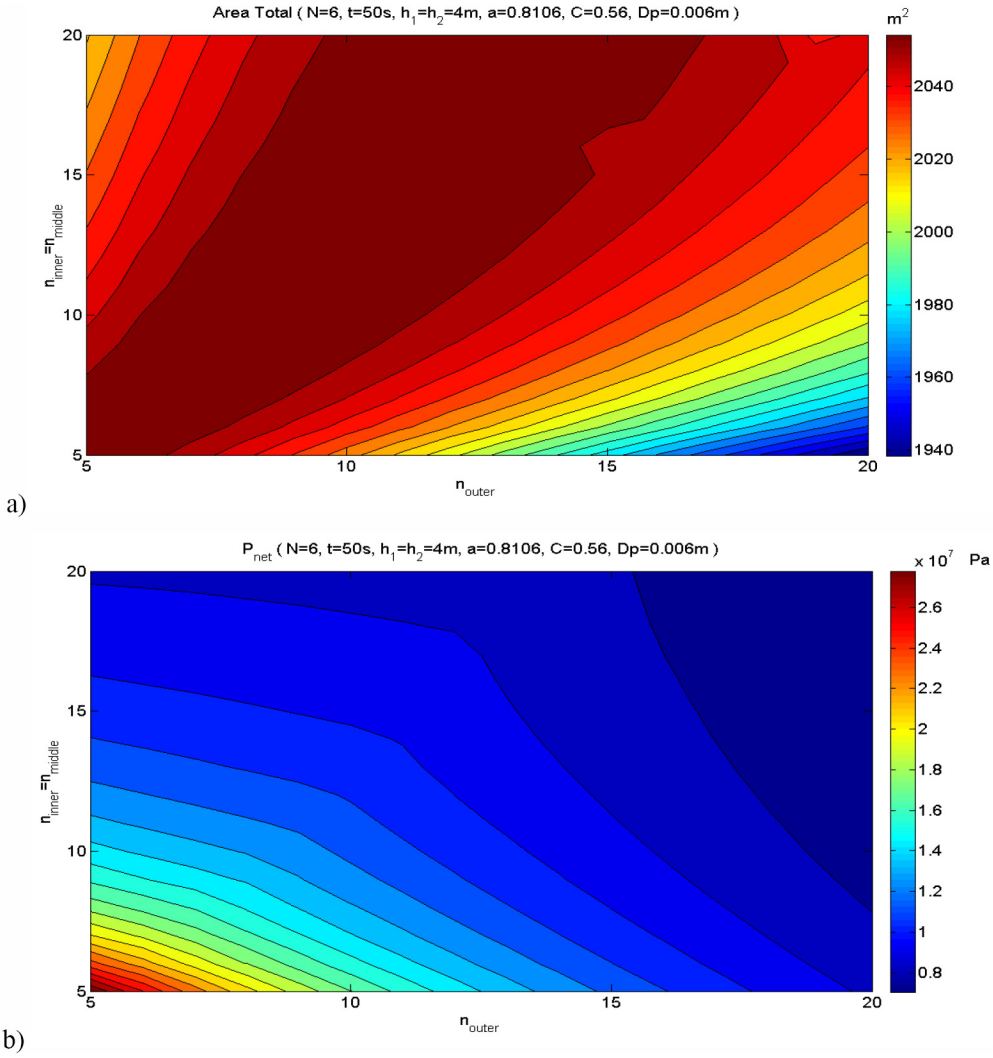

Figure 13—a) Optimization of area for 6 fracture cases at uniform spacing. a) $A(t,h_1,h_2)$ varying with different D_p for fixed n, b) $A(t,h_1,h_2)$ varying with differing n for constant D_p. b) Contours of the corresponding net pressure.

The uniformity of growth can also be compared and contrasted firstly between optimized, non-uniform limited entry design with a case with negligible perforation pressure drop, i.e. no limited entry (Fig. 14a). Clearly the radii of the fractures are more uniform in the optimized case. To further illustrate, Fig. 14b shows a snapshot of the grow of the uniform spacing, no-limited entry case. The suppression of the growth of the central fractures apparent in Fig. 14b is alleviated in the two examples presented in Figs. 14c-d. The former case (Fig. 14c) corresponds to a uniform-spacing but non-uniform limited entry design with n=20 in the central perforation clusters and n=10 for the outer perforations, with D_p=6mm for all (from the top edge in Fig. 13). The latter case (Fig. 14d) corresponds to a uniform spacing and uniform limited entry

design with D_p=6mm and n=5 for all clusters (lower left corner of Fig. 13). Both of these design greatly improve the uniformity of the fracture growth relative to the non-optimized case. They also give a similar result in terms of generated fracture area; the case in Fig. 14d gives 0.2% greater area than Fig. 14c after 50 seconds of growth. However, the required net pressure, recalling Fig. 13b, is substantially different with the non-uniform limited entry case of Fig. 14c requiring 20 MPa (about 3000 psi) less than the comparable uniform limited entry case.

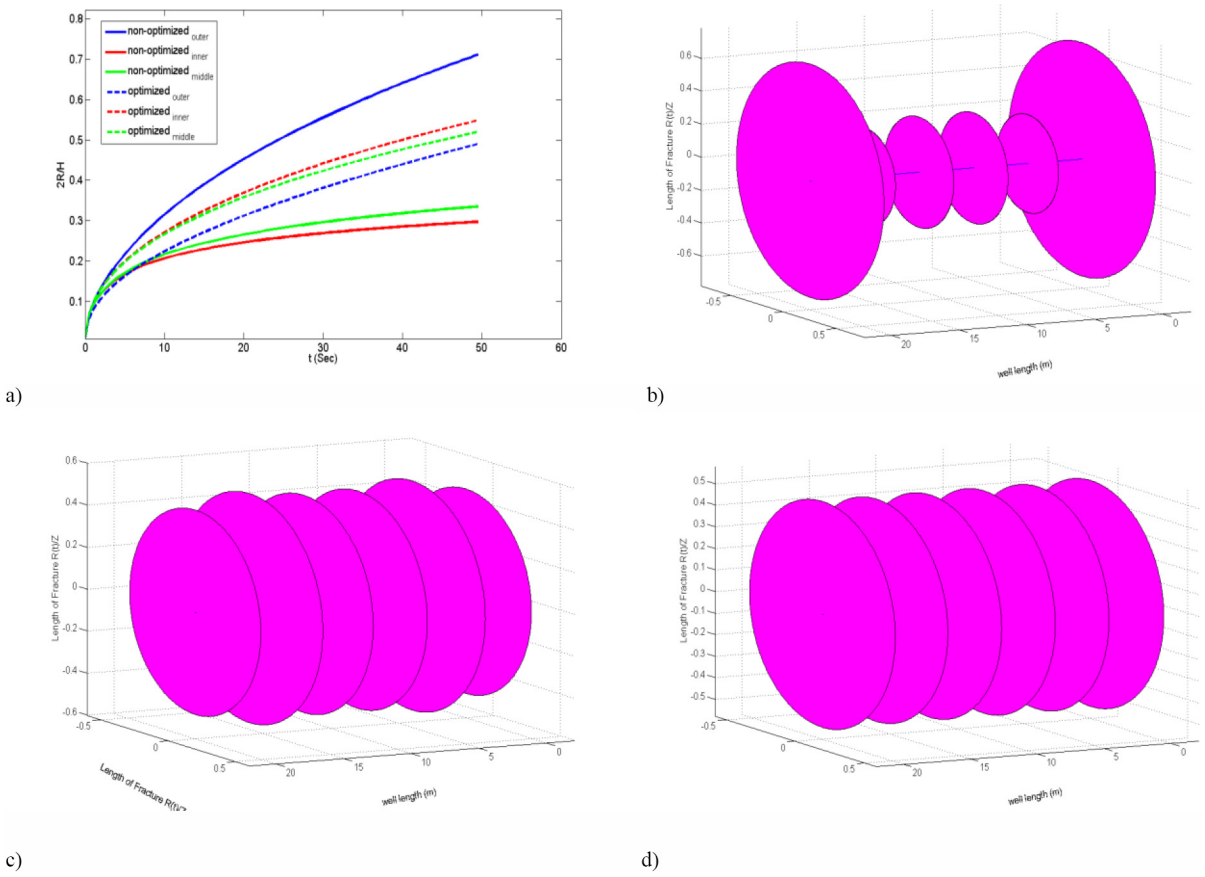

Figure 14—a) Radius of optimized entry design (3D image-b) compared with non-optimized (3D image-c) at the uniform spacing. b) Non-optimized limited entry design. *Dp*(outer)=0.015m, *Dp*(inner)=0.015m, *Dp*(middle)=0.015m, *n*(outer)=20, *n*(inner)=20, *n*(middle)=20, c) Non-uniform limited entry design, Dp(outer)=0.006m, Dp(inner)=0.006m, Dp(middle)=0.006m, n(outer)=10, n(inner)=20, n(middle)=20, d) Uniform limited entry, Dp(outer)=0.006m, Dp(inner)=0.006m, Dp(middle)=0.006m, n(outer)=5, n(inner)=5, n(middle)=5.

Conclusions

The C2Frac model rapidly simulates simultaneous growth of hydraulic fractures, including their mechanical interactions, from multiple perforations in a single stage. For the same numerical experiment, the C2Frac simulation requires only seconds to provide results while the benchmark ILSA model, a fully-coupled planar 3D model, requires days to weeks. However, the C2Frac model only computes over the range for which its salient approximations are relevant, hence, at this point in its development it diverges from the benchmark solution when the hydraulic fractures attain lengths exceeding about 0.6 times the total span of the fracture array, i.e. the stage length. Future efforts will aim to transition to near-field fracture interaction approximations enabling uniform approximation that is not limited. However, even with its current limitations C2Frac is able to demonstrate optimal fracture configurations for generating multiple fracture growth.

The main modeling innovation presented here is the addition of flow through perforations, that is, perforation losses into C2Frac. The impact of the perforations is accounted for via the classical pressure loss model of Crump and Conway (1988), incorporating this result in the global energy balance equation comprising the main coupling equation in the C2Frac model.

For uniform fracture spacing the model confirms the phenomenon of stress shadowing in which growth of one or more fractures is suppressed by the stresses generated by their neighbors. Non-uniform spacing is then shown to be one way to stimulate all hydraulic fractures to grow simultaneously provided the spacing is chosen appropriately (after Peirce and Bunger, 2015), effectively providing a more uniform distribution of stress interactions among the growing hydraulic fractures. From our study, perforation-friction entry is shown to be a complimentary approach, further minimizing the stress shadow effect by properly designing the perforation diameter and number.

The novelty, however, of the results presented here is driven by the rapid computing of C2Frac. Because the simulator takes only seconds to compute (often close to 1 second) on a typical personal computer, thousands of cases were run providing an unprecedented parametric analysis showing combinations of perforation and fracture spacing design leading to maximum fracture uniformity and generated fracture surface area. For example, the parametric study indicates that by choosing smaller perforation diameter and number for the outer clusters, the optimized spacing is closer to uniform at a given treatment time. In addition, such a design, with smaller perforation holes and number at the outer clusters, generates more fracture area at the uniform spacing. However, the results indicate the contrast in perforation friction has to be strong in order to be effective. For the example of a uniform five cluster design, we found optimal results with 5 perforations with 6 mm (~1/4 inches) diameter for the outer clusters and 20 perforations with 15 mm (~5/8 inches) diameter for the inner and middle clusters.

In the end, the results show that limited entry and non-uniform spacing are complimentary approaches. Used together the uniformity and generated fracture surface area are greater than when only one approach is used by itself. Furthermore, when used together the optimal designs can be obtained with closer to uniform spacing and with less drastic contrasts among perforation clusters, both of which are strongly expected to positively impact production relative to designs with less uniformity in the spacing and more drastic differences among perforation clusters.

Future work will firstly be aimed at extending the range of time for which the approximations can be applied by using near-field approximations to the elastic interactions and by including the transition to blade-like fracture growth when/if the radial fractures are limited in growth due to barriers above and below the reservoir. Including fluid leakoff, proppant transport, and connecting the solutions with approximate reservoir simulators are also expected to be straightforward extensions of the current approach. Finally, ongoing research is aimed at testing the modeling and design with laboratory and field experiments.

Acknowledgements

This paper is adapted from a portion of CC's Master's Thesis. Thanks to N. Zolfaghari for his assistance with the Matlab implementation of C2Frac. Thank you also to Xiaowei Weng and Mike Smith for organizing our session and for providing comments on an earlier version of this manuscript.

Nomenclature

E	= Young's Modulus
U	= Elastic Strain Energy
F_f	= Viscous Energy Dissipation
F_c	= Rock Breakage Energy Dissipation
F_{perf}	= Energy Dissipation through Peforations

W_I = Interaction Work
σ_{min} = Minimum In Situ Stress
σ_I = Interaction Stress
t = Pumping Time
μ = Fluid Viscosity
p_f = Fluid Pressure
p_{net} = Fluid Net Pressure
P = Estimator of Fluid Net Pressure
W = Estimator of Fracture Width
Q = Pumping Rate
r = Fluid Density
ν = Poisson's Ratio
n = Number of Perforation Holes in a Cluster
D_p = Perforation Diameter
C = Perforation Shape Factor
a = Perforation Power Loss Coefficient
H = Fracture Height
R = Fracture Radius (Length)
R_w = Wellbore Radius
h = Fracture Spacing
K_{IC} = Rock Fracture Toughness
Z = Stage Length

References

Abass, H. H., M. Y. Soliman, A. M. Tahini, J. Surjaatmadja, D. L. Meadows, and L. Sierra. 2009. Oriented fracturing: A new technique to hydraulically fracture an openhole horizontal well. In Proceedings SPE Annual Technical Conference and Exhibition. New Orleans, LA, USA. SPE 124483.

Bunger, A.P. 2013. Analysis of the power input needed to propagate multiple hydraulic fractures. *International Journal of Solids and Structures* **50,** 1538–1549.

Bunger, A. P., X. Zhang, and R. G. Jeffrey. 2012. Parameters effecting the interaction among closely spaced hydraulic fractures. *Soc. Pet. Eng. J.* **17**(1), 292–306.

Bunger, A. P., R. G. Jeffrey, and X. Zhang. 2014. Constraints on Simultaneous Growth of Hydraulic Fractures from Multiple Perforation Clusters in Horizontal Wells. *SPE Journal,* **19**(4): 608–620.

Cheng C., and A. P. Bunger. In Press. Rapid Simulation of Multiple Radially-Growing Hydraulic Fractures Using an Energy-Based Approach. *Int. J. Numerical Analytical Meth. Geomechanics*. DOI: 10.1002/nag.2471.

Crump J. B., and M. W. Conway. 1988. Effects of perforation-entry friction on bottomhole treating analysis. *J. Pet. Tech,* **40**(8), 1041–1049 (SPE 15474).

Daneshy, A. A. 2015. Dynamic interaction within multiple limited entry fractures in horizontal wells: Theory, implications, and field verification. In SPE Hydraulic Fracturing Technology Conference, The Woodlands, Texas, 3–5 February, SPE 173344.

Economides, M. and Nolte, K.G. 2000. *Reservoir Stimulation,* 3rd edition, New York: John Wiley & Sons, Ltd.

Fisher, M., C. Wright, B. Davidson, A. Goodwin, E. Fielder, W. Buckler, and N. Steinsberger. 2002. Integrating fracture mapping technologies to optimize stimulations in the Barnett Shale. In SPE Annual Technical Conference and Exhibition, San Antonio, Texas, 29 September-2 October, SPE 77441.

Fisher M. K., J. R. Heinze, C. D. Harris, B. M. Davidson, C. A. Wright, and K. P. Dunn. 2004. Optimizing horizontal completion techniques in the Barnett shale using microseismic fracture mapping. In Proceedings SPE Annual Technology Conference and Exhibition. Houston, Texas, USA, 26–29 September, SPE 90051.

Howard, G. C., and C. R. Fast. 1970. *Hydraulic fracturing*. New York, Society of Petroleum Engineers.

Lecampion, B., A. P. Peirce, E. Detournay, X. Zhang, Z. Chen, A. P. Bunger, C. Detournay, J. Napier, S. Abbas, D.

Garagash, and P. Cundall. 2013. The Impact of the Near-Tip Logic on the Accuracy and Convergence Rate of Hydraulic Fracture Simulators Compared to Reference Solutions. In: *Effective and Sustainable Hydraulic Fracturing*. AP Bunger, J McLennan and R Jeffrey (eds.), ISBN 978-953-51-1137-5, (Intech), Chapter 43.

Lecampion, B. and J. Desroches. 2015. Simultaneous initiation and growth of multiple radial hydraulic fractures from a horizontal wellbore. *J. Mech. Phys. Solids* **82,** 235–258.

Lecampion, B., J. Desroches, X. Weng, J. Burghardt, and J. E. Brown. 2015. Can We Engineer Better Multistage Horizontal Completions? Evidence of the Importance of Near-Wellbore Fracture Geometry From Theory, Lab and Field Experiments. SPE Hydraulic Fracturing Technology Conference, The Woodlands, Texas, USA, 3–5 February, SPE 173363.

Nordgren, R. P. 1972. Propagation of a Vertical Hydraulic Fracture. *SPE. J.* **12** (4), 306–314 (SPE 3009).

Meyer, B., and L. Bazan. 2011. A discrete fracture network model for hydraulically induced fractures-theory, parametric and case studies. In Proceedigs SPE Hydraulic Fracturing Technology Conference and Exhibition. The Woodlands, Texas, USA, 24–26 January, SPE 140514.

Miller, C., G. Waters, and E. Rylander. 2011. Evaluation of production log data from horizontal wells drilled in organic shales. In SPE North American Unconventional Gas Conference and Exhibition, The Woodlands, Tx, USA, 14–16 June, SPE 144326.

Peirce, A. P., and A. P. Bunger. 2015. Interference Fracturing: Non-Uniform Distributions of Perforation Clusters that Promote Simultaneous Growth of Multiple Hydraulic Fractures. *Soc. Petroleum Eng. Journal,* **20**(2): 384–395.

Peirce, A. P., and A. P. Bunger. 2014. Robustness of Interference Fractures that Promote Simultaneous Growth of Multiple Hydraulic Fractures. 48th US Rock Mechanics held in Minneapolis, MN, USA, 1–4 June, ARMA-2014-7062.

Peirce, A. P., and E. Detournay. 2008. An implicit level set method for modeling hydraulically driven fractures. *Computer Meth. Appl. Mech. Eng.* **197,** 2858–2885.

Perkins, T.K. and Kern, L.R. 1961. Widths of Hydraulic Fractures. *J. Pet. Tech.* **13** (9): 937–949 (SPE 89).

Roussel, N. P., and M. M. Sharma. 2010. Role of stress reorientation in the success of refracture treatments in tight gas sands. In Proceedings SPE Annual Technical Conference and Exhibition, Florence, Italy. SPE 134491.

Roussel, N. P., and M. M. Sharma. 2011. Optimizing fracture spacing and sequencing in horizontal-well fracturing. *SPE Production & Operations* **26**(2), 173–184.

Savitski, A. A., and E. Detournay. 2002. Propagation of a penny-shaped fluid-driven fracture in an impermeable rock: asymptotic solutions. *Int. J. Solids. Struct.* **39,** 6311–6337.

Sesetty, V., and A. Ghassemi. 2013. Numerical simulation of sequential and simultaneous hydraulic fracturing. In A. P. Bunger, J. McLennan, and R. G. Jeffrey (Eds.), *Effective and Sustainable Hydraulic Fracturing, Chapter 33*. Rijeka, Croatia: Intech.

Warpinski, N., R. C. Kramm, J. R. Heinze, and C. K. Waltman. 2005. Comparison of single-and dual-array microseismic mapping techniques in the Barnett Shale. In SPE Annual Technical Conference and Exhibition, Dallas, Texas, 9–12 October, SPE 95568.

Wu, K. and J. E. Olson. 2013. Investigation of critical in situ and injection factors in multifrac treatments: Guidelines for controlling fracture complexity. In SPE Hydraulic Fracturing Technology Conference, The Woodlands, Texas, 4–6 February, SPE 163821.